Production of tunable circulating tumor cell cluster *in vitro* model via a superhydrophobic microwell array device

By

Olivia Wright

Thesis

Submitted to the Faculty of the

Graduate School of Vanderbilt University

in partial fulfillment of the requirements

for the degree of

MASTER OF SCIENCE

in

Biomedical Engineering

May, 12th, 2023

Nashville, Tennessee

Approved:

Dr. Michael R. King

Dr. John T. Wilson

Acknowledgements

This work was funded by the National Institute of Health National Cancer Institute Grant No. CA256054. C_4F_8 deposition was conducted as part of a user project at the Center for Nanophase Materials Sciences (CNMS), which is a US Department of Energy, Office of Science User Facility at Oak Ridge National Laboratory. Device fabrication and analysis was conducted at the Vanderbilt Institute of Nanoscale Science and Engineering (VINSE) cleanroom and analytical labs. Olivia Wright would like to thank Michael R. King, Maria Lopez Cavestany, and the King Lab members for their support and guidance, Noah Reckhorn and Tin Nguyen for their assistance, Shannon & Eric Wright for their support, and the VINSE and CNMS staff for their guidance.

TABLE OF CONTENTS

List of Tables

Table Page

List of Figures

List of Abbreviations

CTC	Circulating tumor cell
FSS	Fluid shear stress
SHArD	Superhydrophobic array device
ZnO	Zinc oxide
SEM	Scanning electron microscopy
PDI	Polydispersity index
WCA	Water contact angle
F-Actin	Filamentous actin
SD	Standard deviation

Chapter 1: Introduction

Cancer metastasis, often involving the spread of circulating tumor cells (CTCs) to secondary sites in the body, is the leading cause of death in cancer patients [1, 2]. During the metastatic cascade, cancer cells within the primary tumor can undergo epithelial-to-mesenchymal transition (EMT) which allows them to intravasate into the bloodstream [1, 2]. These “circulating tumor cells” (CTCs) travel through the bloodstream, extravasate to a secondary site, and transition back to an epithelial morphology enabling the formation and growth of secondary metastatic lesions [1, 2]. Clinical studies have shown that the presence of CTCs in the peripheral blood can be used as a prognostic factor in cancer patients [3-6]. However, less than 0.1% of CTCs survive the conditions in the bloodstream as they must escape immune attacks and are exposed to high fluid shear stress (FSS) [2, 7].

The presence of CTC aggregates or clusters has also been found in the bloodstream of cancer patients [8, 9]. Clustering is thought to confer metastatic advantage to CTCs, with up to a 50-fold increase in metastatic potential [8, 9]. Clusters can be homotypic, consisting of just tumor cells, or heterotypic, comprised of tumor and non-tumor cells. These non-tumor cells, including cancer associated fibroblasts, immune cells, epithelial cells, and platelets, have been shown to further increase the metastatic potential of CTCs [10-12]. Also, larger CTC clusters may indicate a shorter progression free survival [13]. Understanding how CTC clusters have enhanced survival in the bloodstream would allow us to design better treatments to prevent cancer metastasis. One method to study CTC clusters is by isolation from whole blood. Like capturing single

CTCs, methods for CTC cluster isolation include the use of antibodies and microfluidic devices [14]. An antibody-based method approved by the US FDA, CellSearch, detects CTC clusters that express epithelial cell adhesion molecule (EpCAM) and cytokeratins. However, due to the small surface-area-to-volume ratio of clusters, antibody-based methods have low efficiency [5, 15]. Microfluidic devices have been developed to utilize physical properties such as size to overcome this limitation [16]. One device called the Cluster-Chip has triangular micro-pillar arrays that capture CTC clusters from blood [15]. This method can cause damage to the cells and disaggregation in the process, however, due to the use of turbulent flow [5]. Nonetheless, even if these isolation techniques have high efficiency, they are limited by the low levels of CTC clusters in the bloodstream—less than 10% of CTCs from cancer patients are in cluster form [16-18].

In vitro methods of modeling CTC clusters utilize immortalized cell lines. This method consists in growing cells until they are a confluent monolayer, adding trypsin, and then gently pipetting to not disrupt floating cell aggregates [15, 18, 19]. While they have shown these aggregates show some similarity to primary CTC clusters, there are some drawbacks [18]. The main drawback is that there is no way to control the size of aggregates formed. Additionally, trypsin works by decreasing cell adherence and damages the cell-cell junctions, therefore the cells in the clusters formed are loosely bound [20]. Lastly, modeling heterotypic clusters is very difficult as it is not possible to control the ratio of different cell types in each individual cluster. This Master's thesis focuses on the design of a device to form uniform clusters of cancer cells to study CTC cluster physiology and metastatic advantages. As seen in the overview schematic in

Figure 1, the superhydrophobic array device (SHArD) has a superhydrophobic surface at the bottom of microwells where cancer cells are seeded and grown into cell aggregates.

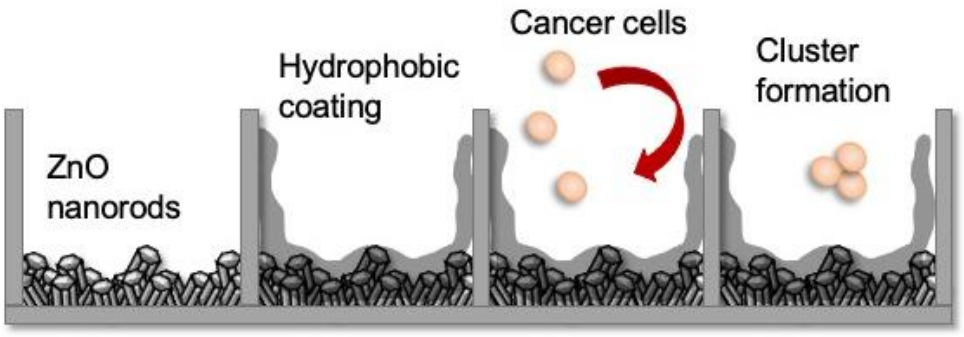

Figure 1. Superhydrophobic array device (SHArD) overview. The superhydrophobic surface consists of ZnO nanorods and a C_4F_8 polymer coating. Cancer cells are seeded into the microwells and form into small aggregates.

The microwell array allows us to culture uniform, size-controlled clusters. Cells interact with surfaces differently based on their wettability [21, 22].Commercial cell culture grade plates are hydrophobic, as they are designed to allow cells to attach and grow in a monolayer. Superhydrophobic surfaces are known to be inert to cell adhesion, compared to hydrophobic and hydrophilic surfaces [23, 24]. There are two essential components to a superhydrophobic surface: nanoscale roughness and a water repellant surface chemistry [25]. These were achieved by a high surface roughness from zinc oxide (ZnO) nanorods coated with a non-sticky polymer. The SHArD successfully produced uniform cell clusters that can be size controlled and withstand physiologically relevant shear stress unlike the clusters from the control method. This novel method of *in vitro* CTC

cluster formation is easily tunable and more reproducible than current methods in the literature and can help better understand the metastatic advantage clustering provides CTCs.

Chapter 2: Materials & Methods

2.1 ZnO thin film deposition and nanorod growth

The zinc oxide nanoparticle solution was prepared using a 15% (w/v) ZnO nanoparticle powder (Zinc oxide NanoTek, 40-100nm APS powder, Alfa Aesar, 44899), MilliQ filtered water, and industrial-grade dispersant Sokalan CP10 (BASF, 50072047) at 1% (w/v). A uniform and monodisperse solution was produced using probe sonication (Sonic Dismembrator Model 100, Fisher Scientific) for 60 s at power level 5 while on ice. The solution was sonicated for durations ranging from 0 to 180 s to determine the optimal duration.

Silicon wafers were prepared for the ZnO layer by cleaning in acetone and performing a plasma cleaning for 5 min using a Trion Phantom II. The ZnO nanoparticle solution was spin coated at 1500 rpm for 30 s onto the silicon wafers, accelerating at 300 rpm/s, and dried at room temperature [26]. Following ZnO thin film deposition, wafers were annealed at 500°C in Argon gas at atmospheric temperature for 1 hr in a 4" tube furnace (MTI OTF-1200X) to enhance the ZnO seed crystallinity [27-29]. To prevent wafer shattering, 40 min heating and cooling steps were included in the annealing protocol.

After annealing, the wafers were placed angled face-down in a 500 mL Teflon-lined autoclave while submerged in a bath of 0.03M zinc nitrate hexahydrate ($Zn(NO_3)_2$) (Sigma Aldrich, 228737-500G), 0.02M hexamethylenetetramine (HMTA) (Sigma Aldrich, 398160-250G), and MilliQ water to grow the nanorods [27, 30]. The nanorod precursor bath solution was prepared at a ratio of 0.67:1 $Zn(NO_3)_2$:HMTA. The wafers were baked for

90°C for 4 hrs in an oven. After the growth process, wafers were washed in MilliQ water and dried overnight under vacuum.

To form the microwell walls, photolithography techniques were used. First, an adhesion promoter called OmniCoat (Kayaku, G112850 0500L 1GL) was deposited onto the wafers seen in Table 1. OmniCoat was spin coated onto the wafers at 3000 rpm for 30 s and baked at 200°C for 1 min. Next, a 75 μm thick grid of SU8 2075 was deposited onto the wafer using the recipe in Table 2. UV Exposure was done with a Karl Suss MA-6 mask aligner. Microwell wall height was confirmed to be 65 μm tall with a profilometer.

Table 1. Omnicoat recipe for SHArD.

	Speed [rpm]	Acceleration [$rpm*s^{-1}$]	Time [s]	Temperature [°C]	Exposure [mJ/cm^2]
Spread	500	100	5	--	--
Spin	3000	300	30	--	--
Bake	--	--	60	200	--

Table 2. SU8 lithography recipe for SHArD microwell walls.

	Speed [rpm]	Acceleration [rpm/s]	Time [s]	Temperature [°C]	Exposure [mJ/cm^2]
Spread	500	100	10	--	--
Spin	3000	300	30	--	--
Softbake 1	--	--	180	65	--
Softbake 2	--	--	540	95	--
Exposure	--	--	--	--	220
Postbake 1	--	--	120	65	--
Postbake 2	--	--	480	95	--
Develop	--	--	420	--	--
Hardbake	--	--	300	180	--

The photolithography mask was designed using the L-Edit software (Siemens) and printed using a Heidelberg Instruments uPG101 laser writer. The mask consists of an array of 70 μm x 70 μm squares spaced 30 μm apart. A CTC is between 16-30 μm, and an average cluster is 2-100 cells [18, 31]. The microwell dimensions are based on these sizes.

The final step in the device fabrication process was to deposit a layer of non-sticky polymer onto the device. First, the wafers were diced to 11 mm x 11 mm squares using a DISCO DAAD3220 dicing saw to fit inside a 24-well cell culture plate. The polymer deposition was completed via C_4F_8 plasma polymerization using an Oxford Instruments PlasmaLab System 100 at the Oak Ridge National Laboratories Center for Nanophase Materials Science cleanroom. This method deposits a highly uniform Teflon-like non-sticky polymer film, lowering surface wettability [32]. The composition can be seen in Table 3.

Table 3. C_4F_8 plasma polymerization composition.

	O_2 [sccm]	C_4F_8 [sccm]	SF_6 [sccm]	HBP [4]	Time [s]	Pressure [mTorr]	HF (fwd) [W]	ICP (fwd) [W]	Temperature [°C]
Step 1: GAS ON	50	10	10	10	10	20	0	0	10
Step 2: STRIKE UP	0	200	10	10	5	20	15	1500	10
Step 3: DEPOSITION	0	200	10	10	20	25	0	2500	10
Step 4: PUMP OUT	0	0	0	0	30	0	0	0	10

2.2 Device Characterization

Scanning electron microscopy was utilized to characterize the device. Samples were sputter coated in gold and imaged using a Zeiss Merlin with Gemini II column. The SU8 height was measured using a Bruker Dektak 150 stylus profilometer using a 12.5 μm tip via contact stylus profilometry mode. To measure static contact angle, a 10 μL drop of DI water was dropped on the surface and imaged using an Ossila Contact Angle Goniometer.

2.3 Cell Culture and Reagents

The metastatic colorectal cancer cell line HCT116 (ATCC, #CCL-247) was cultured in McCoy's 5A cell culture medium (Gibco, 16600-082) supplemented with 10% (v/v) Heat Inactivated Fetal Bovine Serum (Gibco, 16140-071) and 1% (v/v) PenStrep (Gibco, 15140-122-100ML). The prostate carcinoma cell line LNCaP (ATCC #CRL-1740) was cultured in RPMI 1640 cell culture medium (Gibco, 11875-093) supplemented with 10%

(v/v) Fetal Bovine Serum (Gibco, 26140-079), 1% (v/v) PenStrep, 1% (v/v) HEPES Buffer 1M (Corning, 25-060-CI) and 1% (v/v) Sodium Pyruvate 100 mM (Gibco, 11360-070). HCT116 and LNCaP cells were incubated in humidified conditions at 37°C and 5% CO_2 and passaged before exceeding 90% confluency. For passaging, cells were washed in calcium and magnesium free HBSS buffer, lifted with 0.25% trypsin-EDTA (Gibco, 25200-056) for 3 min, and resuspended in complete media before centrifugation at 300 x g for 5 min. The supernatant was removed, and cell pellets were resuspended in complete media.

All experiments were performed in 24-well plates. SHArDs were sterilized under UV light for 45 min prior to cell seeding. SHArDs were placed in the 24-well plate with tweezers. Two mL of complete media was added to each well and pipetted 5-10 times to dispense air bubbles. The 24-well plates are centrifuged at 800 x g for 5 min to remove leftover air bubbles and overcome the tension forces of the superhydrophobic surface. Equation 1 was used to calculate the volume of cell suspension added to each well for the desired number of cells per cell cluster.

$$\frac{cells_m}{SA_m} = \frac{cells_w}{SA_w} \quad (1)$$

Here $cells_m$ is the desired cells per microwell in the SHArD and $cells_w$ is the total number of cells seeded into each well of the 24-well plate. The surface area of the SHArD microwells, SA_m, is 0.0064mm^2 and the 24-well plate wells, SA_w, is 190 mm^2.

Cell clusters have been found to be 2-100 cells/cluster, so the optimized seeding densities were 3, 5, and 7 cells per microwell to get small, medium, and large clusters, respectively [18, 31]. Cells were cultured for 3 doubling times: HCT116 cell clusters were grown for 48 hr and LNCaPs for 72 hr [33, 34]. Cell clusters were harvested from the

SHArDs by pipetting 5-10 times to release the clusters into suspension. As a control, 200,000 cells/well were plated and grown in monolayer form. 0.05% trypsin-EDTA (Gibco, 25300-054) was added at the end point to lift the cells and floating cell clusters were pipetted gently to prevent disaggregation [15, 18, 19].

2.4 Fluid Shear Stress

To model physiologically relevant constant fluid shear stress (FSS) that CTC clusters experience in the bloodstream, Brookfield cone-and-plate viscometers were used via a protocol described previously in Mitchell and King [35]. The cone-and-plate viscometer applies a uniform FSS to the cells in suspension regardless of their distance from the center axis or upper or lower surfaces. The shear rate (G) is given by Equation 2:

$$G = \frac{\omega}{\tan(\theta)} \tag{2}$$

where ω is the cone angular velocity (rad/s) and θ is the angle of the cone (rad). Under experimental conditions, the flow field was assumed to be laminar and fluid was assumed to be Newtonian. The shear stress is given by Equation 3:

$$\tau = \mu G \tag{3}$$

where μ is the viscosity (cP) of the fluid. The viscosity was approximately 3 cP for these experiments. Prior to FSS treatment, the cone-and-plate viscometers were cleaned with 70% ethanol and blocked with 5% bovine serum albumin (BSA) (A1470-100G, Sigma Aldrich) for 1 hr. The BSA solution was removed, and 2 mL of the cell cluster suspension was added to the plates and sheared for 100 RPM (188 s^{-1}) using the CP-41Z spindle for

1 hr with an approximate shear stress of 5 dyne/cm^2. The cell clusters were plated in a 6-well plate for imaging before and after FSS treatment using an Olympus IX81 inverted microscope equipped with a 10x objective. Ten images were randomly taken per sample. Images were processed using ImageJ software. The freehand outline tool was used to find the Feret diameter, or the longest distance across the selection boundary, of single cells and clusters to use to approximate volume. Single cells were assumed to be spherical, and so Equation 4 was used to estimate the volume:

$$V = \frac{4}{3}\pi\left(\frac{f_d}{2}\right)^3 \tag{4}$$

where is r is the Feret diameter divided by 2. Ten single cells were measured. Clusters were approximated to be ellipsoidal, and Equation 5 used to estimate the volume:

$$V = \frac{4}{3}\pi\left(\frac{f_d}{2}\right)\left(\frac{f_m}{2}\right)^2 \tag{5}$$

where f_d is the Feret diameter and f_m is the minimum Feret diameter. Five clusters were analyzed per sample. The number of cells per cluster was determined by dividing the total volume by the average volume of a single cell.

2.5 Confocal Microscopy

Cell clusters were harvested and fixed in 4% (v/v) paraformaldehyde (15714-S, Electron Microscopy Sciences) in DPBS for 15 min, and then permeabilized in 1% (v/v) Triton-X-100 (9002-93-1, Sigma Aldrich) in DPBS for 10 min. Then, clusters were blocked for 2 hr in 10% (v/v) BSA (A1470-100G, Sigma Aldrich) in DPBS and 10% (v/v) normal goat serum (50062Z, Invitrogen). The clusters were incubated overnight at 4°C with 2:100 E-cadherin (24E10) rabbit mAb (3195S, Cell Signaling Technology) in blocking serum.

The next day the cells were incubated with the secondary stain 2:500 Anti-rabbit IgG Fab2 Alexa Fluor(R) 488 (4412S, Cell Signaling Technology) for 2 hr at RT and 2:1000 DAPI (D1306, Invitrogen,) and ActinRedTM 555 ReadyProbesTM reagent (R37112, Invitrogen) cocktail for 30 min at RT in the blocking serum. Washing steps were performed in between each step using HBSS. The stained clusters were spun onto glass slides using a Cytospin 3 (74000102, Shandon) and a drop of antifade mounting media (H-1000, Vectrashield) and coverslips were added.

The slides were imaged using an LSM 900 Zeiss Confocal microscope with a 63x oil immersion objective. Five random images were taken per sample. Image analysis was performed in FIJI using a macro to quantify cell nuclei and E-cadherin fluorescence (Appendix). Briefly, the 'analyze particles' feature was used to count the nuclei on the blue channel (DAPI). The red channel (F-actin) was used to create a binary mask of the cell cluster that was used to measure raw integrated intensity of the green channel (E-cadherin). Three randomly placed squares were used to measure the background intensity. The integrated density was calculated using Equation 6 which subtracts the raw integrated density of the background from the raw integrated density of the cell cluster divided by nuclei count.

$$total\ IntDen = \frac{RawIntDen_c - RawIntDen_b}{nuclei\ count} \quad (6)$$

Chapter 3: Results

3.1 Superhydrophobic array device (SHArD)

This study sought to create an improved method for creating an *in vitro* model of circulating tumor cell clusters (CTCs). Based on cell and material interactions, a superhydrophobic surface would limit cells adhesion to the surface and instead promote cell:cell interactions and binding. The device is designed with an array of microwells to culture small cell aggregates with a wall-to-wall distance of 100 μm and wall depth of 75 μm, as seen in Figure 2A. This wall-to-wall distance was chosen to match expected cluster sizes observed in the blood which range from 2-100 cells [18, 31]; most clusters average around 20 cells per cluster and the average cancer cell is about 20 μm in diameter. The superhydrophobic array device (SHArD) was fabricated using a multi-step additive process outlined in Figure 2B at the Vanderbilt Institute for Nanoscale Science and Engineering and the Oak Ridge Center for Nanophase Material Science cleanrooms.

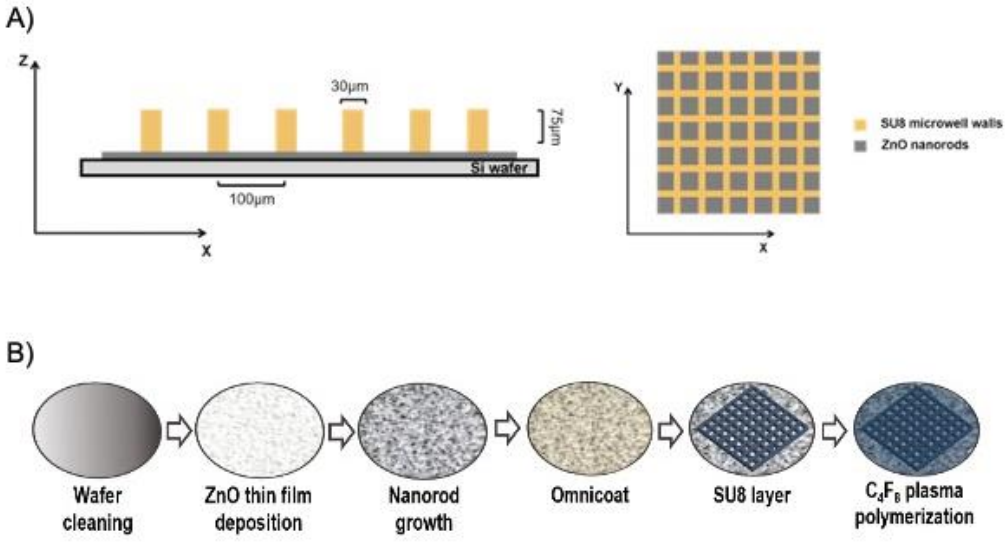

Figure 2. SHArD overview. A) Device design with a wall-to-wall distance of 100 μm, wall thickness of 30 μm and height of 75 μm. B) Device fabrication process outline.

3.2 ZnO nanoparticles create nanoscale surface roughness.

The first part of creating a superhydrophobic surface is nanoscale surface roughness. For this device, we used ZnO nanorods. First, a ZnO nanoparticle solution was spin coated onto silicon wafers. The solution was dispersed using probe sonication, and the effects of different sonication times were analyzed using dynamic light scattering to find the shortest time to create a monodisperse solution. As seen in Figures 3A & 3B, no sonication time had particles with a diameter larger than 1000 nm and a z-avg of 340 ± 60 nm, while sonication times of 30-180 s showed more narrow size distributions and smaller z-avg sizes, with no significant difference between them. The polydispersity index measures the breadth of the molecular weight distribution with a smaller value correlating to a more monodisperse solution. The solution with no sonication time exhibited an average PDI of 0.264 ± 0.046 while sonication times of 30-180 s had PDIs less than 0.14, as seen in Figure 3C. There was a significant difference between the z-avg and PDI of the 60 s time to the control compared to the 30 s time, identifying 60 s sonication time as the optimal condition. Figure 3D shows an even coating of ZnO nanoparticles across a silicon wafer with this sonication time. After depositing the thin film of ZnO nanoparticles, the wafers were annealed and placed in a nanorod growth bath. The SEM image in Figure 3E shows a random assortment of nanorods which creates the high surface

roughness needed for a superhydrophobic surface. The layer was about 1.5 μm thick, seen in Figure 3F, and the nanorods were about 100 μm in diameter Figure 3G.

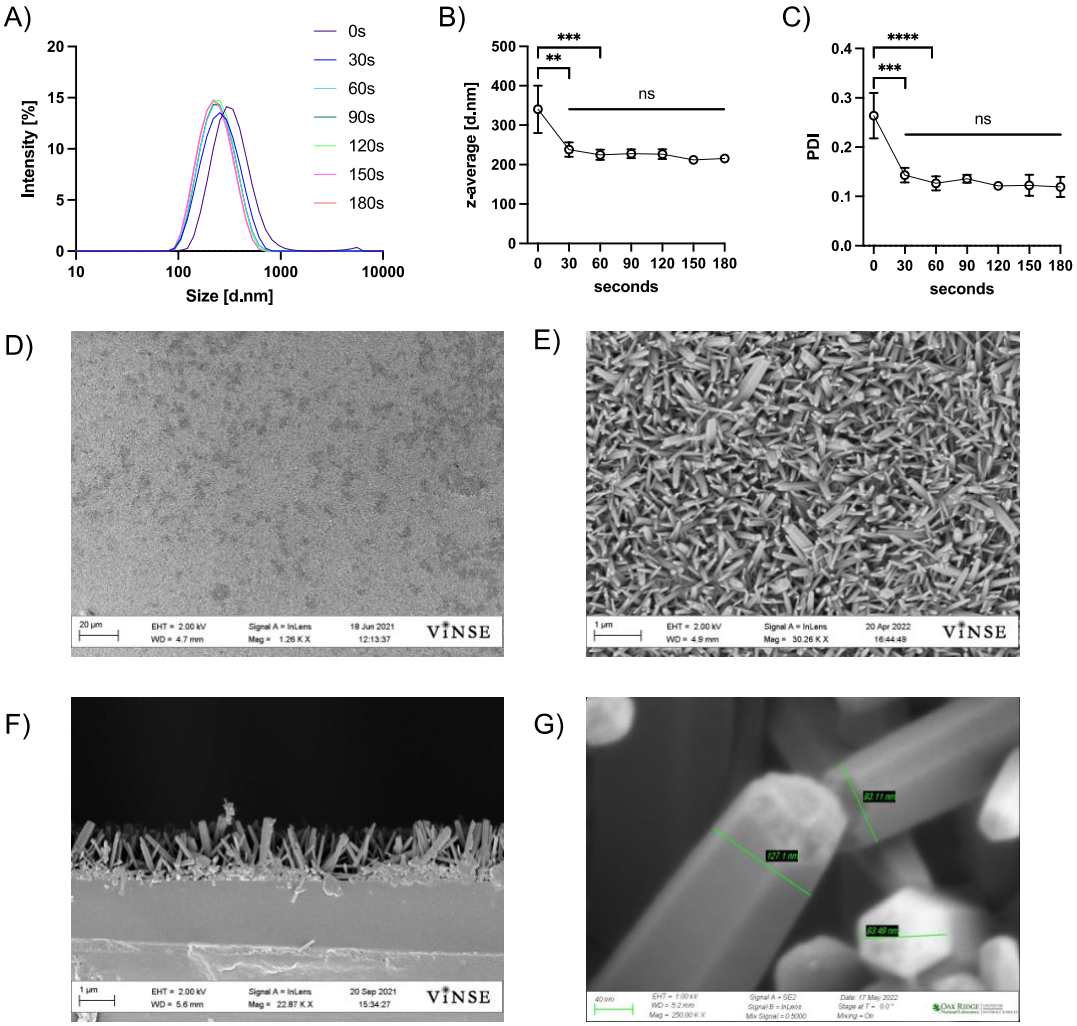

Figure 3. ZnO nanorod layer. A) Size distribution intensity graph of ZnO nanoparticle solution with different sonication times. B) Z-average sizes of ZnO nanoparticles in solution. C) PDI of ZnO nanoparticle solution. Graphs display the mean ± SD for n = 3 sample size. Statistical significance is shown as ** for p<0.01, *** for p<0.001, and **** for p<0.0001, as evaluated by one-way ANOVAs. SEM images showing D) ZnO nanoparticle solution after spin coating, E) ZnO nanorods

after annealing and growth bath, F) side view of nanorod layer, and G) diameter of nanorods.

3.3 Microwell array.

Next, the microwell walls were created with SU8 photoresist using lithography techniques. Figures 4A & 4B shows an even array of microwells. The walls show no tapering seen in Figure 4C from the UV exposure and were confirmed to be about 65 μm tall with the profilometer measurement seen in Figure 4D.

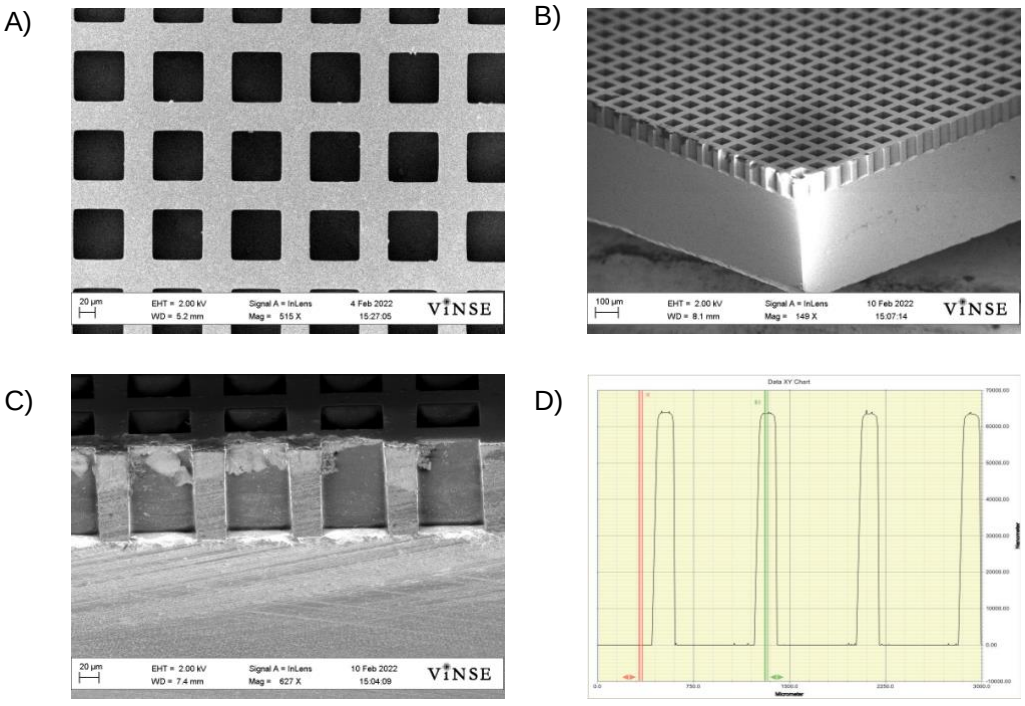

Figure 4. Microwell array. SEM images of A) top view, B) overview, and C) side view of the microwells on the silicon wafer. D) Profilometer measurements of microwell wall height.

3.4 C_4F_8 polymer coating in combination with nanorods produces a superhydrophobic surface.

In addition to a high surface roughness, a hydrophobic coating or non-wetting surface chemistry is needed to create a superhydrophobic surface. For this design, a Teflon-like polymer C_4F_8 was deposited using a reactive ion etcher. First, the silicon wafers were diced to 11 x 11 mm chips seen in Figure 5A to fit inside a 24-well plate for cell culture. The devices were then placed on a carrier wafer for the polymer deposition. The gas polymerization recipe yielded a thin film of polymer seen in Figure 5B where the high surface roughness is still observed. Water contact angle (WCA) measurements were used to confirm the creation of a superhydrophobic surface with a WCA>150° correlating to a superhydrophobic surface. The blank silicon wafer with the C_4F_8 polymer yielded a WCA of 115° while the combination of nanorods with the polymer yielded a WCA of 167°.

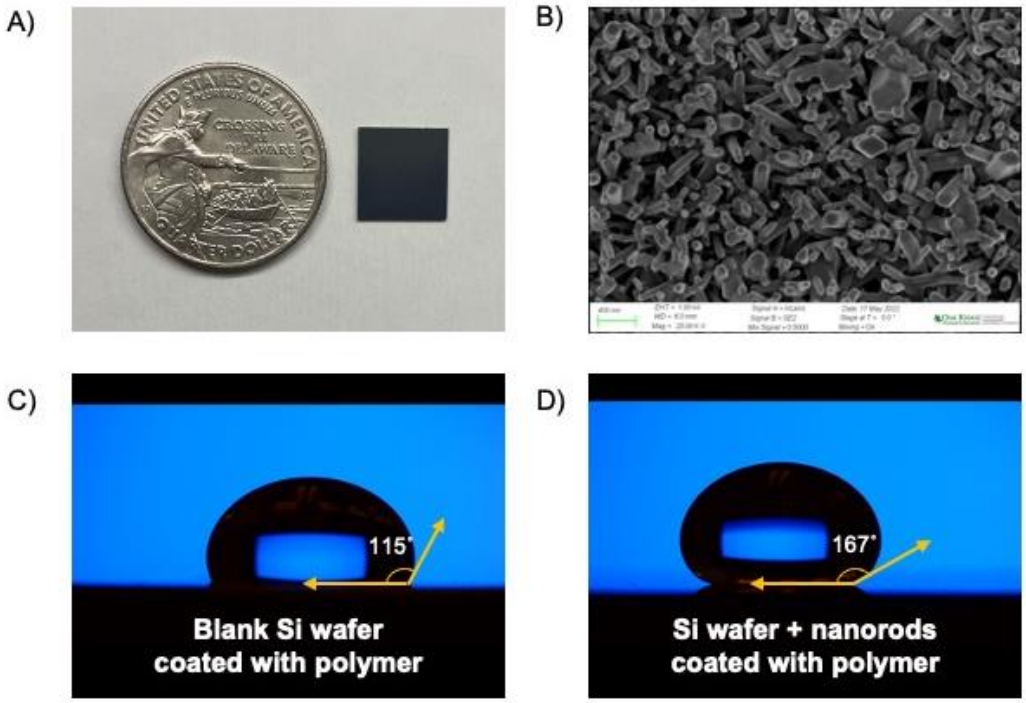

Figure 5. Non-sticky polymer coating. A) 11mm x 11mm diced SHArD next to a quarter. B) SEM image of C_4F_8 polymer coating. WCA measurements of C) blank silicon wafer coated with the polymer and D) silicon wafer with the nanorods coated with the polymer.

3.5 Cell clusters grown in the SHArD have a tunable size and remain clustered under physiological FSS better than the control method.

One of the major limitations with the current monolayer method for forming cell aggregates *in vitro* is that there is no control of cell cluster size. The SHArD allows control of size based on the number of cells seeded per well. The average size of cell clusters found in the bloodstream range from 2-100 cells, and this guided range of cluster sizes tested [15, 18, 19]. 3, 5, and 7 cells were seeded per microwell of the SHArD to grow small, medium, and large clusters, respectively. Representative images of the control and the LNCaP cell clusters grown with the SHArD can be seen in Figure 6A. The number of cells per cluster was calculated by dividing the volume of the cluster (Equation 5) by the volume of a single cell (Equation 4). There was a stepwise increase in sizes of the clusters grown in the SHArD based on seeding density and low standard deviations compared to the control method (Figures 6B). The control method produces clusters of random sizes with an average of 102.0 ± 82.8 cells per cluster. The SHArD produced small, medium, and large clusters with 20.4 ± 9.2, 32.3 ± 10.1, and 63.5 ± 19.4 cells per cluster, respectively. Notably, the standard deviation of the control cluster sizes was significantly larger than that of all 3 clusters grown in the SHArD, confirming that our device can reproducibly control cluster size (Figures 6C).

Then, we tested how the clusters would respond to physiologically relevant fluid shear stress (FSS) they might experience in the bloodstream. The clusters were harvested and placed in cone-and-plate viscometers for 1 h at 188 s^{-1} and imaged before and after shear exposure (Figure 6D). The number of cells per cluster was calculated as in prior measurements. The control method showed a 68.3% decrease in cluster size whereas the clusters grown in the SHArD had no significant difference in cluster size, as seen in Figure 6E.

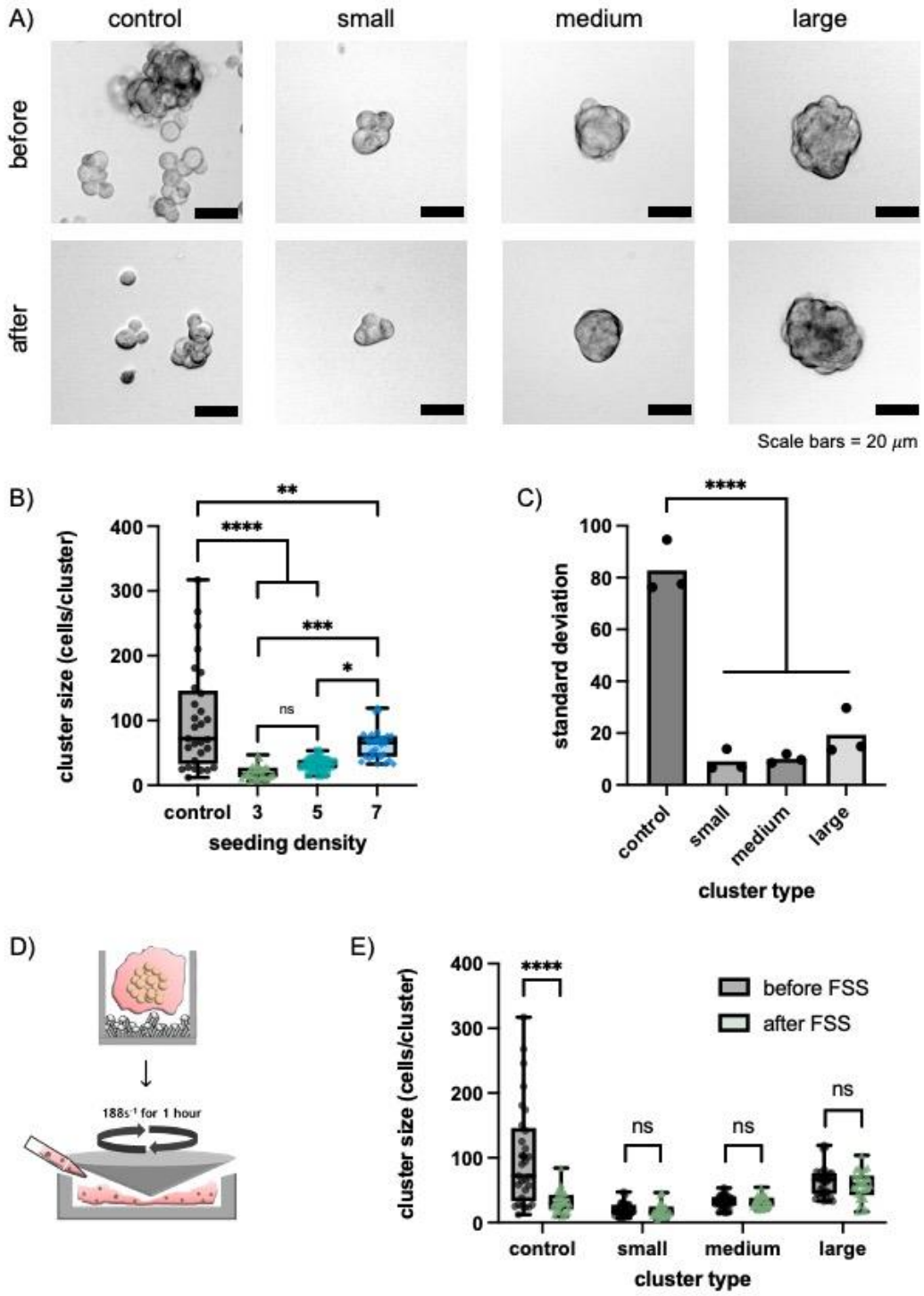
A)
control
small
medium
large
before
after
Scale bars = 20 μm
B)
cluster size (cells/cluster)
400
300
200
100
0
**
****
***
*
ns
control
3
5
7
seeding density
C)
****
standard deviation
100
80
60
40
20
0
control
small
medium
large
cluster type
D)
188s⁻¹ for 1 hour
E)
cluster size (cells/cluster)
400
300
200
100
0
****
ns
ns
ns
before FSS
after FSS
control
small
medium
large
cluster type

Figure 6. LNCaP cell clusters grown in the SHArD have a tunable size and remain clustered under physiological FSS better than using the control method. A) Brightfield representative images of the LNCaP cell clusters before and after experiencing FSS. Scale bars = 20 μm B) Cell cluster sizes based on seeding density. C) Standard deviation of the cell cluster sizes. D) Overview of FSS experiment. E) Cell cluster sizes before and after experiencing FSS. Graphs display the mean ± SD. Statistical significance is shown as * for $p<0.05$, ** for $p<0.01$, *** for $p<0.001$, and **** for $p<0.0001$, as evaluated by one-way ANOVAs.

HCT116 cell clusters responded similarly. The SHArD produced small, medium, and large clusters with 21.6 ± 12.4, 50.6 ± 27.0, and 83.1 ± 34.5 cells per cluster, respectively. The control method produced smaller clusters compared to the LNCaP cell clusters and showed a lower standard deviation at 29.1 ± 23.2 cells per cluster; however, they still had the highest percentage decrease with 68.4% decrease compared to the SHArD clusters with less than a 20% decrease.

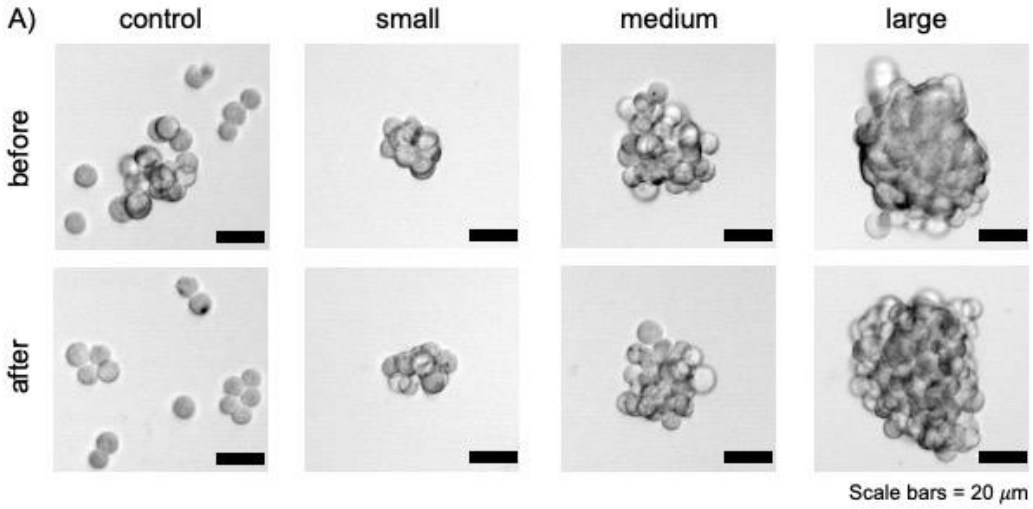
A)
control
small
medium
large
before
after
Scale bars = 20 μm

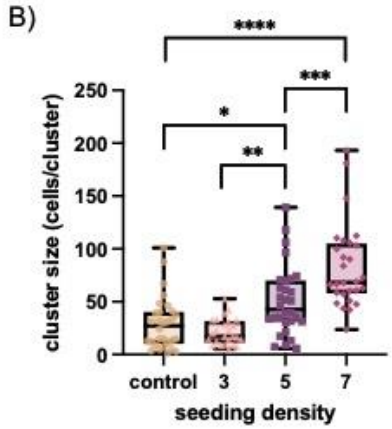
B)
****
***
*
**
cluster size (cells/cluster)
250
200
150
100
50
0
control
3
5
7
seeding density

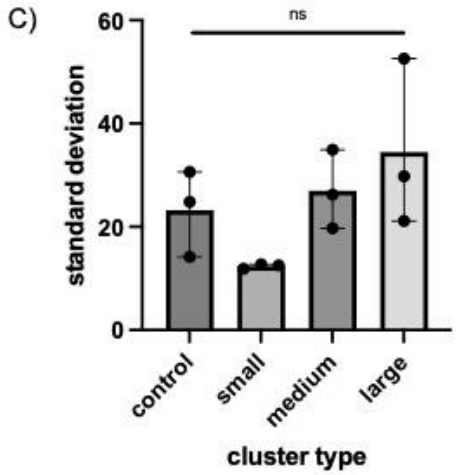
C)
ns
standard deviation
60
40
20
0
control
small
medium
large
cluster type

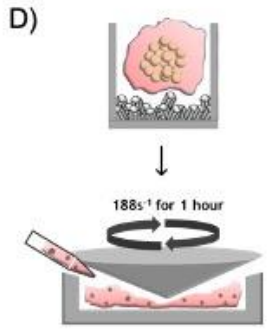
D)
188s⁻¹ for 1 hour

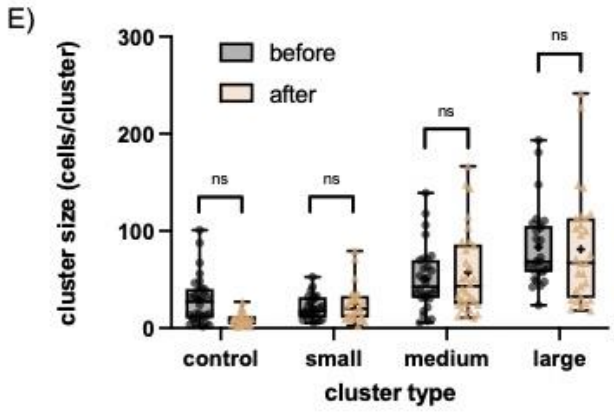
E)
before
after
ns
ns
ns
ns
cluster size (cells/cluster)
300
200
100
0
control
small
medium
large
cluster type

Figure 7. HCT116 cell clusters grown in the SHArD have a tunable size and remain clustered under physiological FSS better than using the control method. A) Brightfield representative images of the HCT116 cell clusters before and after experiencing FSS. Scale bars = 20 μm. B) Cell cluster sizes based on seeding density. C) Standard deviation of the cell cluster sizes. D) Overview of FSS experiment. E) Cell cluster sizes before and after experiencing FSS. Graphs display the mean ± SD. Statistical significance is shown as * for $p<0.05$, ** for $p<0.01$, *** for $p<0.001$, and **** for $p<0.0001$, as evaluated by one-way ANOVAs.

3.6 Cell clusters grown in the SHArD have increased E-cadherin expression.

The protein adhesion molecule E-cadherin was examined via confocal microscopy. E-cadherin is a protein involved in cell-cell adhesions in epithelial cells and can affect cell proliferation, migration, cell polarization, and survival [36]. E-cadherin can have tumor-suppressing and tumor-promoting functions depending on the cancer cell's role in the metastatic cascade [36]. However, E-cadherin has been shown to contribute to CTC cluster survival through anoikis and FSS resistance [8, 37, 38]. Consistent with the results from the FSS data (Figures 6 & 7), the cell clusters grown in the SHArD showed increased E-cadherin expression compared to the control cell clusters (Figures 8 & 9). The LNCaP SHArD cell clusters showed a 20-40% increase in E-cadherin expression compared to the control samples and the HCT116 SHArD cell clusters showed a 70-90% increase.

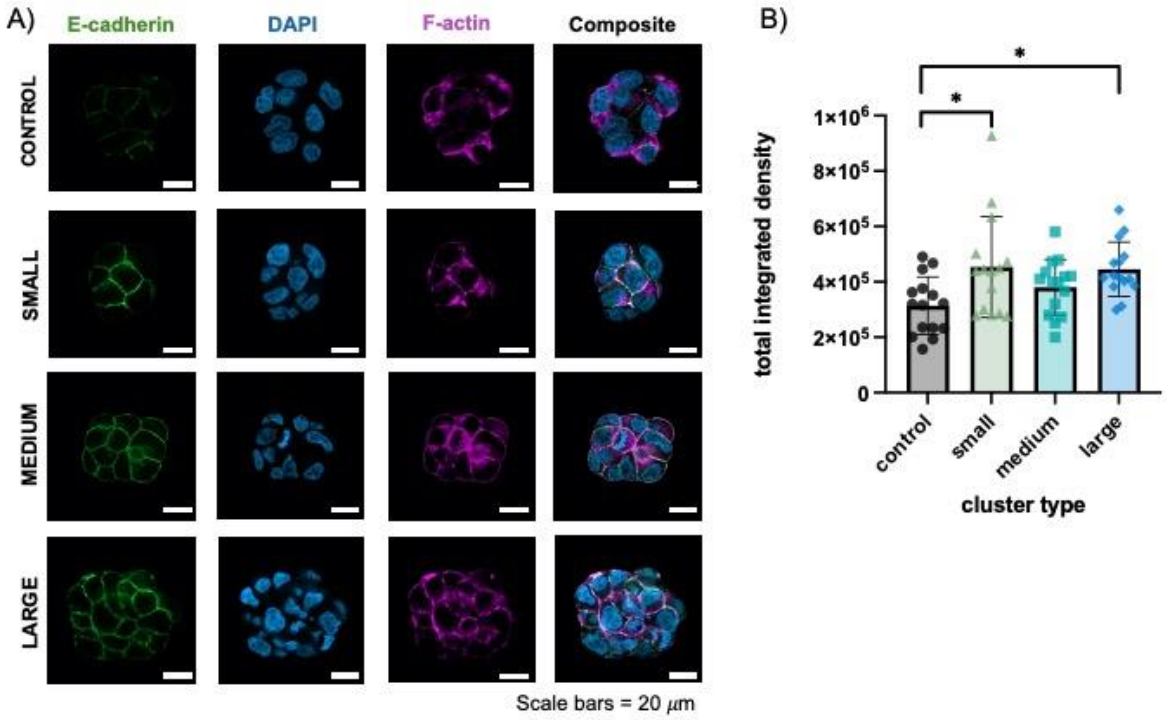

Figure 8. LNCaP cell clusters grown in the SHArD have increased E-cadherin expression. A) Confocal representative images of the LNCaP cell clusters stained for E-cadherin, DAPI, and F-actin. Scale bars = 20 μm. B) Quantification of the total integrated density of E-cadherin. Graphs display the mean ± SD. Statistical significance is shown as * for $p<0.05$ as evaluated by one-way ANOVAs.

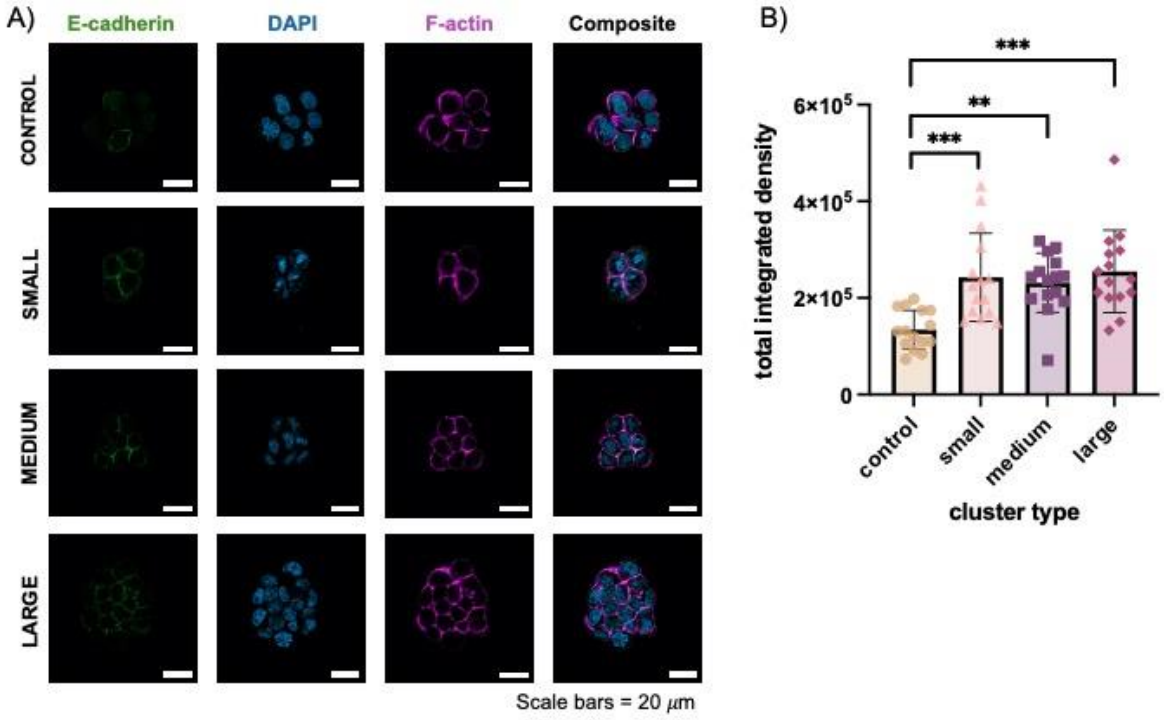

Figure 9. HCT116 cell clusters grown in the SHArD have increased E-cadherin expression. A) Confocal representative images of the HCT116 cell clusters stained for E-cadherin, DAPI, and F-actin. Scale bars = 20 μm. B) Quantification of the total integrated density of E-cadherin. Statistical significance is shown as ** for $p<0.01$, *** for $p<0.001$ as evaluated by one-way ANOVAs.

Chapter 4: Conclusions

In this study, a superhydrophobic array device (SHArD) was designed for an *in vitro* model of circulating tumor cell (CTC) clusters. A combination of ZnO nanorods and C_4F_8 polymer coating created a superhydrophobic surface with a WCA of 167°. LNCaP and HCT116 cell lines were used to evaluate the efficiency of the device. The microwell array created uniform, reproducible cell clusters with tunable sizes based on seeding density compared to the control that produced a more variable range of sizes. The cell clusters grown in the SHArD remained clustered after experiencing physiological fluid shear stress better than the control clusters. Moreover, the SHArD clusters showed increased E-cadherin expression through confocal imaging, indicating stronger cell-to-cell adhesion. The cell clusters grown with this device can serve as a better model to study the metastatic advantage clustering provides CTCs.

References

[1] D. Hanahan and Robert, "Hallmarks of Cancer: The Next Generation," *Cell,* vol. 144, no. 5, pp. 646-674, 2011, doi: 10.1016/j.cell.2011.02.013.

[2] X. Zhong *et al.*, "Circulating tumor cells in cancer patients: developments and clinical applications for immunotherapy," *Molecular Cancer,* vol. 19, no. 1, 2020, doi: 10.1186/s12943-020-1141-9.

[3] N. N. Rahbari *et al.*, "Meta-analysis shows that detection of circulating tumor cells indicates poor prognosis in patients with colorectal cancer," *Gastroenterology,* vol. 138, no. 5, pp. 1714-1726. e13, 2010.

[4] A. Romiti *et al.*, "Circulating tumor cells count predicts survival in colorectal cancer patients," (in eng), *J Gastrointestin Liver Dis,* vol. 23, no. 3, pp. 279-84, Sep 2014, doi: 10.15403/jgld.2014.1121.233.arom1.

[5] Y. Hong, F. Fang, and Q. Zhang, "Circulating tumor cell clusters: What we know and what we expect (Review)," *International Journal of Oncology,* vol. 49, no. 6, pp. 2206-2216, 2016, doi: 10.3892/ijo.2016.3747.

[6] Z. Mu *et al.*, "Prospective assessment of the prognostic value of circulating tumor cells and their clusters in patients with advanced-stage breast cancer," *Breast Cancer Research and Treatment,* vol. 154, no. 3, pp. 563-571, 2015, doi: 10.1007/s10549-015-3636-4.

[7] J. M. Barnes, J. T. Nauseef, and M. D. Henry, "Resistance to Fluid Shear Stress Is a Conserved Biophysical Property of Malignant Cells," *PLOS ONE,* vol. 7, no. 12, p. e50973, 2012, doi: 10.1371/journal.pone.0050973.

[8] N. Aceto *et al.*, "Circulating Tumor Cell Clusters Are Oligoclonal Precursors of Breast Cancer Metastasis," *Cell,* vol. 158, no. 5, pp. 1110-1122, 2014, doi: 10.1016/j.cell.2014.07.013.

[9] J.-M. Hou *et al.*, "Circulating Tumor Cells as a Window on Metastasis Biology in Lung Cancer," *The American Journal of Pathology,* vol. 178, no. 3, pp. 989-996, 2011, doi: 10.1016/j.ajpath.2010.12.003.

[10] D. G. Duda *et al.*, "Malignant cells facilitate lung metastasis by bringing their own soil," *Proceedings of the National Academy of Sciences,* vol. 107, no. 50, pp. 21677-21682, 2010, doi: 10.1073/pnas.1016234107.

[11] N. Ortiz-Otero, A. B. Clinch, J. Hope, W. Wang, C. A. Reinhart-King, and M. R. King, "Cancer associated fibroblasts confer shear resistance to circulating tumor cells during prostate cancer metastatic progression," (in eng), *Oncotarget,* vol. 11, no. 12, pp. 1037-1050, Mar 24 2020, doi: 10.18632/oncotarget.27510.

[12] D. Sharma, K. E. Brummel-Ziedins, B. A. Bouchard, and C. E. Holmes, "Platelets in tumor progression: a host factor that offers multiple potential targets in the treatment of cancer," *Journal of cellular physiology,* vol. 229, no. 8, pp. 1005-1015, 2014.

[13] Z. Li *et al.*, "Analysis of the prognostic role and biological characteristics of circulating tumor cell-associated white blood cell clusters in non-small cell lung cancer," *Journal of Thoracic Disease,* vol. 14, no. 5, p. 1544, 2022.

[14] Z. Deng, S. Wu, Y. Wang, and D. Shi, "Circulating tumor cell isolation for cancer diagnosis and prognosis," *eBioMedicine,* vol. 83, p. 104237, 2022, doi: 10.1016/j.ebiom.2022.104237.

[15] A. F. Sarioglu *et al.*, "A microfluidic device for label-free, physical capture of circulating tumor cell clusters," *Nature Methods,* vol. 12, no. 7, pp. 685-691, 2015, doi: 10.1038/nmeth.3404.
[16] C. Macaraniag, Q. Luan, J. Zhou, and I. Papautsky, "Microfluidic techniques for isolation, formation, and characterization of circulating tumor cells and clusters," *APL Bioengineering,* vol. 6, no. 3, p. 031501, 2022, doi: 10.1063/5.0093806.
[17] N. Ortiz-Otero *et al.*, "TRAIL-coated leukocytes to kill circulating tumor cells in the flowing blood from prostate cancer patients," *BMC Cancer,* vol. 21, no. 1, 2021, doi: 10.1186/s12885-021-08589-8.
[18] A. N. May, B. D. Crawford, and A. M. Nedelcu, "In vitro model-systems to understand the biology and clinical significance of circulating tumor cell clusters," *Frontiers in Oncology,* vol. 8, p. 63, 2018.
[19] S. H. Au *et al.*, "Clusters of circulating tumor cells traverse capillary-sized vessels," *Proceedings of the National Academy of Sciences,* vol. 113, no. 18, pp. 4947-4952, 2016, doi: 10.1073/pnas.1524448113.
[20] H.-L. Huang *et al.*, "Trypsin-induced proteome alteration during cell subculture in mammalian cells," *Journal of biomedical science,* vol. 17, no. 1, pp. 1-10, 2010.
[21] H. G. Xie *et al.*, "Effect of surface wettability and charge on protein adsorption onto implantable alginate-chitosan-alginate microcapsule surfaces," *Journal of Biomedical Materials Research Part A: An Official Journal of The Society for Biomaterials, The Japanese Society for Biomaterials, and The Australian Society for Biomaterials and the Korean Society for Biomaterials,* vol. 92, no. 4, pp. 1357-1365, 2010.
[22] Y. Arima and H. Iwata, "Effect of wettability and surface functional groups on protein adsorption and cell adhesion using well-defined mixed self-assembled monolayers," *Biomaterials,* vol. 28, no. 20, pp. 3074-3082, 2007/07/01/ 2007, doi: https://doi.org/10.1016/j.biomaterials.2007.03.013.
[23] M. Ferrari, F. Cirisano, and M. C. Morán, "Mammalian Cell Behavior on Hydrophobic Substrates: Influence of Surface Properties," *Colloids and Interfaces,* vol. 3, no. 2, p. 48, 2019, doi: 10.3390/colloids3020048.
[24] Y. Yuan, M. P. Hays, P. R. Hardwidge, and J. Kim, "Surface characteristics influencing bacterial adhesion to polymeric substrates," *RSC advances,* vol. 7, no. 23, pp. 14254-14261, 2017.
[25] C. Mao *et al.*, "Preparation of lotus-leaf-like polystyrene micro- and nanostructure films and its blood compatibility," *Journal of Materials Chemistry,* vol. 19, no. 47, p. 9025, 2009, doi: 10.1039/b912314h.
[26] J. A. Alvarado, A. Maldonado, H. Juarez, and M. Pacio, "Synthesis of colloidal ZnO nanoparticles and deposit of thin films by spin coating technique," *Journal of Nanomaterials,* vol. 2013, pp. 167-167, 2013.
[27] R. Parize, J. Garnier, O. Chaix-Pluchery, C. Verrier, E. Appert, and V. Consonni, "Effects of Hexamethylenetetramine on the Nucleation and Radial Growth of ZnO Nanowires by Chemical Bath Deposition," *The Journal of Physical Chemistry C,* vol. 120, no. 9, pp. 5242-5250, 2016, doi: 10.1021/acs.jpcc.6b00479.
[28] M. Fiedot, I. Maliszewska, O. Rac-Rumijowska, P. Suchorska-Woźniak, A. Lewińska, and H. Teterycz, "The relationship between the mechanism of zinc

oxide crystallization and its antimicrobial properties for the surface modification of surgical meshes," *Materials,* vol. 10, no. 4, p. 353, 2017.
[29] A. Joraid, A. Solieman, M. Al-Maghrabi, and M. Almutairy, "Studies of crystallization kinetics and optical properties of ZnO films prepared by sol–gel technique," *Journal of Sol-Gel Science and Technology,* vol. 97, pp. 523-539, 2021.
[30] K. Yoo *et al.*, "Low-temperature large-area fabrication of ZnO nanowires on flexible plastic substrates by solution-processible metal-seeded hydrothermal growth," *Nano Convergence,* vol. 7, pp. 1-10, 2020.
[31] I. Martínez-Pena *et al.*, "Dissecting Breast Cancer Circulating Tumor Cells Competence via Modelling Metastasis in Zebrafish," *International Journal of Molecular Sciences,* vol. 22, no. 17, p. 9279, 2021, doi: 10.3390/ijms22179279.
[32] M. Iqbal, D. K. Dinh, Q. Abbas, M. Imran, H. Sattar, and A. Ul Ahmad, "Controlled surface wettability by plasma polymer surface modification," *Surfaces,* vol. 2, no. 2, pp. 349-371, 2019.
[33] G. Li, C. Nelsen, and E. A. Hendrickson, "Ku86 is essential in human somatic cells," *Proceedings of the National Academy of Sciences,* vol. 99, no. 2, pp. 832-837, 2002, doi: doi:10.1073/pnas.022649699.
[34] A. s. M. Ballangrud, W.-H. Yang, A. Dnistrian, N. M. Lampen, and G. Sgouros, "Growth and Characterization of LNCaP Prostate Cancer Cell Spheroids1," *Clinical Cancer Research,* vol. 5, no. 10, pp. 3171s-3176s, 1999.
[35] M. J. Mitchell and M. R. King, "Fluid shear stress sensitizes cancer cells to receptor-mediated apoptosis via trimeric death receptors," *New Journal of Physics,* vol. 15, 2013, doi: 10.1088/1367-2630/15.
[36] J.-H. Venhuizen, F. J. C. Jacobs, P. N. Span, and M. M. Zegers, "P120 and E-cadherin: Double-edged swords in tumor metastasis," *Seminars in Cancer Biology,* vol. 60, pp. 107-120, 2020/02/01/ 2020, doi: https://doi.org/10.1016/j.semcancer.2019.07.020.
[37] M. Maeshiro *et al.*, "Colonization of distant organs by tumor cells generating circulating homotypic clusters adaptive to fluid shear stress," *Scientific Reports,* vol. 11, no. 1, 2021, doi: 10.1038/s41598-021-85743-z.
[38] L. A. Hapach *et al.*, "Phenotypic Heterogeneity and Metastasis of Breast Cancer Cells," *Cancer Research,* vol. 81, no. 13, pp. 3649-3663, 2021, doi: 10.1158/0008-5472.Can-20-1799.

Appendix

Fiji macro for E-cadherin measurement:

```
// CHOOSE THE DIRECTORIES FOR THE IMAGE FILES AND RESULT STORAGE

waitForUser("Choose folder where the images are, and second where you want to store the data tables");
directory1 = getDirectory("Choose the Directory");
//directory2 = getDirectory("Choose the Directory");
list1 = getFileList(directory1);
//print(list.length);

run("Set Measurements...", "area mean integrated redirect=None decimal=3");

// IMAGE ANALYSIS FOR E-CADHERIN FLUORESCENCE
    for (i=0; i<list1.length; i++) {

    //Open dapi
    filepath = "open=[" + directory1 + list1[i] + "] color_mode=Colorized rois_import=[ROI manager] split_channels view=Hyperstack stack_order=XYCZT series_1";
            run("Bio-Formats Importer", filepath);
```

```
//Remove empty channels
deleteimage1 = list1[i] + " - C=0";
close(deleteimage1);
deleteimage1 = list1[i] + " - C=1";
close(deleteimage1);

//count nuclei
setAutoThreshold("Default dark");
run("Threshold...");
//waitForUser("set threshold");

setThreshold(20, 255);
setOption("BlackBackground", false);
run("Convert to Mask");
run("Analyze Particles...", "size=10-Infinity display clear summarize add");

//savetable = directory2 + list1[i] + " dapi_count.txt";
//saveAs("Results", savetable);

roiManager("Delete");
//Table.deleteRows(0, 0, "Results");
//close(savetable);
```